

Hyperfine-induced effects on the $K\alpha_1$ angular distribution following electron-impact excitation of heliumlike spin-1/2 Tl^{79+} ions

Z. W. Wu^{1,*}, Z. Q. Tian,¹ J. Jiang,¹ C. Z. Dong,¹ and S. Fritzsche^{2,3}

¹Key Laboratory of Atomic and Molecular Physics & Functional Materials of Gansu Province, College of Physics and Electronic Engineering, Northwest Normal University, Lanzhou 730070, People's Republic of China

²Helmholtz-Institute Jena, Fröbelstieg 3, D-07743 Jena, Germany

³Theoretisch-Physikalisches Institut, Friedrich-Schiller-Universität Jena, Max-Wien-Platz 1, D-07743 Jena, Germany



(Received 24 October 2021; accepted 14 December 2021; published 27 December 2021)

Angular distribution of the $K\alpha_1$ ($1s2p\ ^{1,3}P_{1,2} \rightarrow 1s^2\ ^1S_0$) emission line following electron-impact excitation of heliumlike spin-1/2 Tl^{79+} ions is studied within the framework of the density-matrix theory and the relativistic distorted-wave theory. In particular, we aim to explore how a (nonzero) nuclear magnetic dipole moment μ_I affects the $K\alpha_1$ angular distribution due to the hyperfine interactions. To this end, detailed calculations are performed for selected spin-1/2 $^A_{81}\text{Tl}^{79+}$ ($A = 187, 205, \text{ and } 207$) ions with large μ_I . It is found that the hyperfine-induced effects on the $K\alpha_1$ angular distribution depend strongly on the impact electron energy. When compared with the case of zero-spin Tl^{79+} ions, the $K\alpha_1$ angular distribution becomes much more anisotropic for low impact energies, whereas this anisotropy decreases quickly at intermediate and high impact energies. Such a behavior is in sharp contrast to the results for the fine-structure-resolved $1s2p\ ^3P_2 \rightarrow 1s^2\ ^1S_0$ component [Phys. Rev. A **102**, 042813 (2020)]. Therefore, accurate $K\alpha_1$ angular measurements at low impact electron energies could be employed as a sensitive tool to probe the hyperfine interaction in highly charged few-electron ions.

DOI: 10.1103/PhysRevA.104.062814

I. INTRODUCTION

When one of the K -shell ($1s$) electrons of atoms or ions is excited to some unoccupied subshells or simply ionized, the subsequent radiative decay by filling the K -shell vacancy with one of the L -shell $2p$ electrons gives rise to well-known characteristic $K\alpha$ spectral lines. During the past few decades, indeed, various $K\alpha$ -relevant studies have been performed both theoretically and experimentally. In early times, these studies were primarily focused on relative intensities of $K\alpha$ (satellite) lines with respect to the corresponding $K\beta$ lines [1–5], various physical and chemical effects on $K\alpha$ intensities and energies [6–12], assignments [13], yields [14,15], energy shifts [15–17], line shapes [18], and linewidths [19–21] of $K\alpha$ lines. Furthermore, $K\alpha$ lines were found to be a potential efficient x-ray source [22,23] and employed as an effective tool to diagnose astrophysical and (proton- and laser-produced) laboratory plasmas [24–28], determine the site of oxygen in boron suboxides [29], and explore production mechanism of spectral lines [30]. Moreover, $K\alpha$ lines radiated from iron ions also attracted much attention due to their particular significance in astrophysics [31–37]. With rapid development of x-ray spectrometers, both accuracy and resolution have been substantially improved. Such a substantial improvement has stimulated a great deal of high-precision theoretical and experimental studies relevant to $K\alpha$ lines, such as accurate determination of $K\alpha$ transition energies and rates and line

strengths [38–43], radiative properties of subshell-resolved $K\alpha_{1,2}$ components [44–46] and so on.

Besides total transition properties of $K\alpha$ lines, their angle- and polarization-resolved properties, such as angular distribution and linear polarization have been also attracting much attention from atomic physicists. For example, the linear polarization of $K\alpha$ photons radiated from heliumlike Sc^{19+} ions was measured at the Lawrence Livermore electron-beam ion trap [47]. Moreover, both the linear polarization [48] and angular distribution [49–51] of $K\alpha_1$ lines following the radiative electron capture (REC) into initially hydrogenlike ions with nonzero nuclear spin were also explored. Recently, we studied the angular distribution of the fine-structure-resolved component $1s2p\ ^3P_2 \rightarrow 1s^2\ ^1S_0$ of $K\alpha_1$ lines following the electron-impact excitation (EIE) of spin-1/2 Tl^{79+} ions by using the relativistic multiconfigurational Dirac-Fock (MCDF) method and relativistic distorted-wave (RDW) theory [52]. In contrast to the results for zero-spin Tl^{79+} ions, the angular distribution was found to be much less anisotropic at all impact energies considered due to the hyperfine interaction.

Since thallium has many relatively stable spin-1/2 isotopes with large nuclear magnetic dipole moment, in this contribution we follow our previous work [52] and investigate further the EIE of heliumlike zero-spin and spin-1/2 Tl^{79+} ions from their ground-state $1s^2\ ^1S_0$ to two excited fine-structure energy levels $1s2p\ ^{1,3}P_{1,2}$ and the subsequent $K\alpha_1$ ($1s2p\ ^{1,3}P_{1,2} \rightarrow 1s^2\ ^1S_0$) radiative decay within the framework of the density-matrix theory and the RDW theory. Special attention is paid, in particular, to the hyperfine-induced effects on the angular distribution of the $K\alpha_1$ lines radiated from these spin-1/2 ions. To this aim, we first calculate the partial EIE cross sections

*zhongwen.wu@nwnu.edu.cn

for excitations to the individual magnetic substates of the two fine-structure energy levels of Ti^{79+} ions for a series of impact electron energies. These partial EIE cross sections are further used to obtain the alignment parameters of the energy levels $1s2p\ ^{1,3}P_{1,2}$ as well as their corresponding hyperfine-structure $1s2p\ ^1P_1$, $F=1/2, 3/2$ and $1s2p\ ^3P_2$, $F=3/2, 5/2$ levels. By means of these alignment parameters and relevant hyperfine transition amplitudes, the effective anisotropy parameters and angular distribution of the $K\alpha_1$ lines are finally obtained. It is found that the hyperfine-induced effects on the $K\alpha_1$ angular distribution depend strongly on the impact electron energy. At low impact energies, for example, the hyperfine interaction makes the $K\alpha_1$ angular distribution of the spin-1/2 ions much more anisotropic when compared with the one of the corresponding zero-spin Ti^{79+} ions, whereas such hyperfine-induced effects on the $K\alpha_1$ angular distribution decrease quickly with increasing impact electron energy and vanish at intermediate and high impact energies. Moreover, it is also found that the $K\alpha_1$ angular distribution behaves insensitively to the magnetic dipole moment of the spin-1/2 Ti^{79+} ions, which is remarkably different from the angular distribution of the magnetic-quadrupole $1s2p\ ^3P_2 \rightarrow 1s^2\ ^1S_0$ lines following the EIE of spin-1/2 Ti^{79+} ions [52] and the $K\alpha_1$ angular distribution following the REC of initially hydrogenlike spin-1/2 Sn^{49+} , Xe^{53+} , and Ti^{80+} ions [49,50].

The rest of this paper is structured as follows. In the following section, the theoretical method is presented in detail for studying the angular distribution of the $K\alpha_1$ lines following the EIE of heliumlike ions with nuclear spin $I=0$ or $1/2$. In Sec. III, we then discuss the obtained alignment parameters of the fine-structure $1s2p\ ^1P_1$ and 3P_2 energy levels as well as their corresponding hyperfine-structure levels and, especially, illustrate in detail the hyperfine-induced effects on the angular distribution of the $K\alpha_1$ lines. Finally, a summary of the present work is made in Sec. IV. Atomic units are used throughout this paper unless specified.

II. THEORETICAL METHOD

In theoretical studies of polarization and angular correlation of (x-ray) photons radiated from atoms or ions following various atomic collision processes with electrons or photons, density-matrix theory can give rise to the most convenient and concise description [53]. To obtain the angular distribution of the $K\alpha_1$ lines radiated from heliumlike ions with nuclear spin $I=1/2$, let us begin with the angular distribution of photons radiated from an arbitrary radiative transition $\alpha_i J_i \rightarrow \alpha_f J_f + \gamma$ of atoms or ions. Within the density-matrix theory, the angular distribution of the γ photons reads as [51,53]

$$\begin{aligned} \mathcal{W}_{J_i J_f}(\theta) &= \frac{1}{4\pi} \left(1 + \sum_{k=2}^{2J_i} \mathcal{A}_k(\alpha_i J_i) f_k(\alpha_i J_i, \alpha_f J_f) P_k(\cos \theta) \right) \\ &= \frac{1}{4\pi} \left(1 + \sum_{k=2}^{2J_i} \beta_k(\alpha_i J_i, \alpha_f J_f) P_k(\cos \theta) \right). \end{aligned} \quad (1)$$

Here, J_i and J_f are total angular momenta of the initial and final energy levels of the transition, whereas α_i and α_f denote all other quantum numbers required for a unique specification of the levels. $\mathcal{A}_k(\alpha_i J_i)$ refers to the so-called alignment param-

eters, which describe the (relative) population of the magnetic substates $|\alpha_i J_i M_i\rangle$ of the excited level $\alpha_i J_i$ and are fully determined by the excitation process. $f_k(\alpha_i J_i, \alpha_f J_f)$ denotes the structure functions reflecting the shell structure of the initial and final levels. $\beta_k(\alpha_i J_i, \alpha_f J_f) \equiv \mathcal{A}_k(\alpha_i J_i) f_k(\alpha_i J_i, \alpha_f J_f)$ is the so-called anisotropy parameters. Moreover, $P_k(\cos \theta)$ is a set of Legendre polynomials with the polar angle θ of the γ photon emission with respect to the quantization z axis. In practice, however, as the fourth- and even higher-rank alignment parameters are much smaller than the second-rank parameter \mathcal{A}_2 [49,54], in what follows only the quantities with $k=2$ in Eq. (1) will be included.

For heliumlike ions with $I=0$, the $K\alpha_1$ line consists of two fine-structure-resolved components $1s2p\ ^1P_1 \rightarrow 1s^2\ ^1S_0$ and $1s2p\ ^3P_2 \rightarrow 1s^2\ ^1S_0$ and, thus, the corresponding $K\alpha_1$ angular distribution can be given by a weighted average over both of them as follows:

$$\mathcal{W}_{K\alpha_1}(\theta) = \mathcal{N}_{E1} \mathcal{W}_{E1}(\theta) + \mathcal{N}_{M2} \mathcal{W}_{M2}(\theta). \quad (2)$$

In this expression, \mathcal{N}_{E1} and \mathcal{N}_{M2} represent the weights of the electric-dipole ($E1$) $1s2p\ ^1P_1 \rightarrow 1s^2\ ^1S_0$ and magnetic-quadrupole ($M2$) $1s2p\ ^3P_2 \rightarrow 1s^2\ ^1S_0$ components, respectively, which are determined by the corresponding total cross sections for populating the excited levels and the branching ratios for the radiative decays to the ground state $1s^2\ ^1S_0$. For the presently considered Ti^{79+} ions, the radiative branching ratio of the $1s2p\ ^1P_1$ level to the ground state reaches 99.9%, whereas the one of the $1s2p\ ^3P_2$ level is determined to be just 77.3%. These branching ratios will affect more or less the $K\alpha_1$ angular distribution in competition with the total cross sections, depending on the impact electron energy used. $\mathcal{W}_{E1}(\theta)$ and $\mathcal{W}_{M2}(\theta)$ denote the respective angular distribution of the components, which can be parametrized to the form of Eq. (1) but with the explicit anisotropy parameters [49,55],

$$\beta_2(^1P_1 \rightarrow ^1S_0) = \frac{\sqrt{2}}{2} \mathcal{A}_2(^1P_1), \quad (3)$$

and

$$\beta_2(^3P_2 \rightarrow ^1S_0) = -\sqrt{\frac{5}{14}} \mathcal{A}_2(^3P_2), \quad (4)$$

respectively, in which $\mathcal{A}_2(^1P_1)$ and $\mathcal{A}_2(^3P_2)$ refer to the second-rank alignment parameters of the $1s2p\ ^1P_1$ and $1s2p\ ^3P_2$ levels, respectively. If the levels are solely populated by the EIE of heliumlike ions, these alignment parameters can be given by means of the partial EIE cross sections as follows [49,54]:

$$\mathcal{A}_2(^1P_1) = \sqrt{2} \frac{\sigma_{|1,1\rangle} - \sigma_{|1,0\rangle}}{2\sigma_{|1,1\rangle} + \sigma_{|1,0\rangle}}, \quad (5)$$

and

$$\mathcal{A}_2(^3P_2) = -\sqrt{\frac{10}{7}} \frac{\sigma_{|2,0\rangle} + \sigma_{|2,1\rangle} - 2\sigma_{|2,2\rangle}}{\sigma_{|2,0\rangle} + 2\sigma_{|2,1\rangle} + 2\sigma_{|2,2\rangle}}. \quad (6)$$

Here, $\sigma_{|1,0\rangle}$ and $\sigma_{|1,1\rangle}$ denote the partial cross sections for the EIE from the ground state to the magnetic substates $|1, 0\rangle$ and $|1, 1\rangle$ of the excited $1s2p\ ^1P_1$ level, whereas $\sigma_{|2,M\rangle}$ with $M=0, 1$, and 2 have a similar meaning but for the substates $|2, M\rangle$ of the $1s2p\ ^3P_2$ level, respectively. In the present paper, these partial EIE cross sections are calculated with the RDW

theory [56,57]. Since the RDW theory has been described in many places, here we will not present the details of it but just recommend readers refer to our relevant work [58–61].

By using Eqs. (1)–(6), one can readily obtain the effective anisotropy parameter $\beta_2^{\text{eff}}(K\alpha_1; I=0)$ of the $K\alpha_1$ line radiated from heliumlike zero-spin ions,

$$\beta_2^{\text{eff}}(K\alpha_1; I=0) = \frac{\sqrt{2}}{2} \mathcal{N}_{E1} \mathcal{A}_2(^1P_1) - \sqrt{\frac{5}{14}} \mathcal{N}_{M2} \mathcal{A}_2(^3P_2). \quad (7)$$

As seen from Eq. (1), once the effective anisotropy parameter $\beta_2^{\text{eff}}(K\alpha_1; I=0)$ is known, the corresponding $K\alpha_1$ angular distribution would be fully determined.

For heliumlike spin-1/2 ions, each of the two fine-structure components of the corresponding $K\alpha_1$ line consists of two hyperfine-resolved $1s2p\ ^1P_1, F_i=1/2, 3/2 \rightarrow 1s^2\ ^1S_0, F_f=1/2$ and $1s2p\ ^3P_2, F_i=3/2, 5/2 \rightarrow 1s^2\ ^1S_0, F_f=1/2$ components, respectively. Nevertheless, since the lifetime of the $1s2p\ ^1P_1$ level is much shorter than the hyperfine interaction time [62], the angular distribution of the fine-structure component $1s2p\ ^1P_1 \rightarrow 1s^2\ ^1S_0$ is not affected by the hyperfine interaction and, hence, is still given by the anisotropy parameter (3). For the $1s2p\ ^3P_2 \rightarrow 1s^2\ ^1S_0$ component, however, the corresponding angular distribution should be given by a weighted summation over the angular distributions of the two hyperfine-resolved $1s2p\ ^3P_2, F_i=3/2, 5/2 \rightarrow 1s^2\ ^1S_0, F_f=1/2$ components, i.e.,

$$\mathcal{W}_{M2}^{\text{hf}}(\theta) = \frac{2}{5} \mathcal{W}_{F_i=3/2}(\theta) + \frac{3}{5} \mathcal{W}_{F_i=5/2}(\theta). \quad (8)$$

Note that the statistical weights 2/5 and 3/5 are used. The angular distributions $\mathcal{W}_{F_i=3/2}$ and $\mathcal{W}_{F_i=5/2}$ have the form of Eq. (1) but with the respective anisotropy parameters [51,52],

$$\beta_2(F_i=3/2 \rightarrow F_f=1/2) = \frac{a_{E1}^{\text{hf}}(\mu_I)^2 + 2\sqrt{3}a_{E1}^{\text{hf}}(\mu_I)a_{M2} - a_{M2}^2}{2[a_{E1}^{\text{hf}}(\mu_I)^2 + a_{M2}^2]} \mathcal{A}_2(F_i=3/2), \quad (9)$$

and

$$\beta_2(F_i=5/2 \rightarrow F_f=1/2) = -\sqrt{\frac{2}{7}} \mathcal{A}_2(F_i=5/2). \quad (10)$$

In writing down Eqs. (9) and (10), for the hyperfine-resolved $1s2p\ ^3P_2, F_i=3/2 \rightarrow 1s^2\ ^1S_0, F_f=1/2$ component both the leading $M2$ and hyperfine-induced $E1$ channels are included, whereas for the $1s2p\ ^3P_2, F_i=5/2 \rightarrow 1s^2\ ^1S_0, F_f=1/2$ component only the $M2$ decay channel is considered and the higher-multipole $E3$ channel is neglected. Here, $\mathcal{A}_2(F_i=3/2)$ and $\mathcal{A}_2(F_i=5/2)$ represent the (second-order) alignment parameters of the hyperfine-structure levels $1s2p\ ^3P_2, F_i=3/2$ and $1s2p\ ^3P_2, F_i=5/2$, respectively. If the hyperfine interaction is incorporated only via the I - J coupling but does not influence the prior EIE process, the alignment parameters $\mathcal{A}_2(\alpha_i J_i I F_i)$ of the hyperfine-structure level $\alpha_i J_i I F_i$ can be expressed in terms of the alignment parameter $\mathcal{A}_2(\alpha_i J_i)$ of the corresponding fine-structure level as follows [48,49]:

$$\mathcal{A}_2(\alpha_i J_i I F_i) = (-1)^{J_i + I F_i} [J_i, F_i]^{1/2} \begin{Bmatrix} F_i & F_i & 2 \\ J_i & J_i & I \end{Bmatrix} \mathcal{A}_2(\alpha_i J_i), \quad (11)$$

where $[a, b] \equiv (2a+1)(2b+1)$ and the standard notation for the Wigner-6j symbols has been utilized. Moreover, a_{M2} and $a_{E1}^{\text{hf}}(\mu_I)$ refer to the reduced transition amplitudes for the leading $M2$ and hyperfine-induced $E1$ decay channels of the hyperfine-resolved $1s2p\ ^3P_2, F_i=3/2 \rightarrow 1s^2\ ^1S_0, F_f=1/2$ component. Obviously, $a_{E1}^{\text{hf}}(\mu_I)$ depends explicitly on the nuclear magnetic dipole moment μ_I . As these reduced amplitudes occur frequently in the studies of radiative properties of atoms or ions, here we just follow our previous work [49,52,54] and will not show the details of them.

By following the same routes for deriving Eq. (7), the effective anisotropy parameter $\beta_2^{\text{eff}}(K\alpha_1; I=1/2)$ can be readily obtained for the $K\alpha_1$ line radiated from heliumlike spin-1/2 ions,

$$\begin{aligned} \beta_2^{\text{eff}}(K\alpha_1; I=1/2) &= \frac{\sqrt{2}}{2} \mathcal{N}_{E1} \mathcal{A}_2(^1P_1) + \frac{2}{5} \sqrt{\frac{7}{5}} \mathcal{N}_{M2} \mathcal{A}_2(^3P_2) \\ &\times \left(\frac{\sqrt{2}}{4} \frac{a_{E1}^{\text{hf}}(\mu_I)^2 + 2\sqrt{3}a_{E1}^{\text{hf}}(\mu_I)a_{M2} - a_{M2}^2}{a_{E1}^{\text{hf}}(\mu_I)^2 + a_{M2}^2} - \frac{3\sqrt{2}}{7} \right). \end{aligned} \quad (12)$$

Once the effective anisotropy parameter $\beta_2^{\text{eff}}(K\alpha_1; I=1/2)$ becomes known, again, the corresponding $K\alpha_1$ angular distribution would be fully determined by using an analog of Eq. (1).

In the present paper, all of the required wave functions and energy levels of heliumlike Ti^{79+} ions are obtained by employing the GRASP92 package based on the relativistic MCDHF method [63,64]. The partial and total EIE cross sections are calculated with the use of the RDW package REIR06 developed by us [65]. Concerning the required reduced amplitudes of the hyperfine-resolved transitions, they are evaluated by means of the RATIP package [66,67]. To be detailed, the configurations $1s^2, 1s2s, 1s2p, 1s3s, 1s3p,$ and $1s3d$ are used to generate the wave functions and binding energies. Nevertheless, the purities of the two energy levels $1s2p\ ^1P_1$ and $1s2p\ ^3P_2$ of interest are extremely high, i.e., achieving 0.999 999 987 and 0.999 999 995, respectively. Such purities indicate that the electron-electron correlation effects are negligibly small. Moreover, the contributions of the Breit interaction and quantum-electrodynamical effects to the wave functions and binding energies are also incorporated, which have been proven to be very important to highly charged ions [68,69]. In the calculations of the EIE cross sections, the Breit interaction is included as well and partial waves of the impact electrons are considered up to a maximum $\kappa = \pm 50$, which is enough to ensure the calculations convergent according to our test calculations. The reduced amplitudes are calculated with the perturbative approach [48,49]. In contrast to nonperturbative approaches, such as the complex matrix method [70,71] and the radiation-damping method [71–73], the perturbative approach does not take the widths of energy levels involved into account, nevertheless, which does not matter for the presently considered case. The reasons are given as follows. The line $1s2p\ ^1P_1 \rightarrow 1s^2\ ^1S_0$ has been known to be hardly affected by the hyperfine interaction and, thus, there is no need to calculate the reduced amplitudes

TABLE I. Presently calculated transition energies and rates for the $1s2p\ ^1P_1 \rightarrow 1s^2\ ^1S_0$ and $1s2p\ ^3P_2 \rightarrow 1s^2\ ^1S_0$ lines of heliumlike Ti^{79+} ions together with other theoretical results available from Głowacki [74] and Drake [75] for comparison. The present results and the ones from Głowacki are calculated within the length gauge. It should be noted that the transition rate $3.148 \times 10^{16}\ \text{s}^{-1}$ is given by converting the original absorption oscillator strength 0.3876 in Ref. [74].

Transitions	Transition energies (eV)			Transition rates (s^{-1})	
	Present	Ref. [74]	Ref. [75]	Present	Ref. [74]
$1s2p\ ^1P_1 \rightarrow 1s^2\ ^1S_0$	74750.078	74708.769	74543.69	3.180×10^{16}	3.148×10^{16}
$1s2p\ ^3P_2 \rightarrow 1s^2\ ^1S_0$	74689.160	74651.121		7.253×10^{13}	

of its hyperfine components, although the level $1s2p\ ^1P_1$ has a large width 20.941 eV that is comparable in size to the separation 60.919 eV between the two levels $1s2p\ ^1P_1$ and $1s2p\ ^3P_2$. Moreover, other energy levels corresponding to the configuration $1s2p$ either have negligibly tiny widths or are very far apart from the two levels and, thus, hardly affect the required reduced amplitudes of the hyperfine-resolved component $1s2p\ ^3P_2, F_i=3/2 \rightarrow 1s^2\ ^1S_0, F_f=1/2$ when the perturbative approach is employed.

III. RESULTS AND DISCUSSION

The presently calculated transition energies and rates for the $1s2p\ ^1P_1 \rightarrow 1s^2\ ^1S_0$ and $1s2p\ ^3P_2 \rightarrow 1s^2\ ^1S_0$ lines of heliumlike Ti^{79+} ions are tabulated in Table I together with other theoretical results available from Głowacki [74] and Drake [75] for comparison. It should be noted that the transition rate $3.148 \times 10^{16}\ \text{s}^{-1}$ is given by converting the original absorption oscillator strength 0.3876 in Ref. [74]. As seen from the table, the present transition energies and transition rates agree very well with the results from Głowacki [74] and the maximum discrepancies are within 0.06% and 1%, respectively, although the results from both Głowacki [74] and us differ obviously from the result of Drake [75]. Such a good agreement indicates that the wave functions and energy levels employed in the present calculations are reliable.

In Fig. 1, we plot the presently calculated partial and total EIE cross sections for the $\varepsilon e + 1s^2\ ^1S_0 \rightarrow 1s2p\ ^{1,3}P_{1,2} + \varepsilon' e$ processes of Ti^{79+} ions as functions of impact electron energy. Note that the impact energies are given in units of the excitation threshold 74.7501 keV of the $1s2p\ ^1P_1$ level, above which both the $1s2p\ ^{1,3}P_{1,2}$ levels can be populated simultaneously. At the threshold, moreover, the impact energy is artificially increased by 0.1 eV in order to avoid difficulties resulting from scattered electrons with zero kinetic energy as we did in Ref. [52]. The symbol “ $M = 0$ ” denotes the partial cross sections for the EIE from the ground state $1s^2\ ^1S_0$ to the magnetic substate $|M = 0\rangle$ of the $1s2p\ ^{1,3}P_{1,2}$ levels, whereas the ones “ $M = \pm 1$ ” and “ $M = \pm 2$ ” have similar meanings. The partial cross sections for the substate $|M = +1\rangle$ of both the levels are fully equal to the ones for the respective substate $|M = -1\rangle$ due to a spatial symmetry of the substates $|M = \pm 1\rangle$, which holds also for the substates $|M = \pm 2\rangle$ of the $1s2p\ ^3P_2$ level. Overall, the presently obtained energy-dependent tendency of both the partial and total cross sections corresponding to the level $1s2p\ ^1P_1$ of Ti^{79+} ions agrees very well with the available results of Au^{77+} ions for the case without the Breit interaction included [77].

As can be seen clearly from the figure, both the partial and the total cross sections corresponding to the $1s2p\ ^1P_1$ level behave quite differently from the ones to the level $1s2p\ ^3P_2$. Within the impact energies considered, the total cross sections for the EIE to the level $1s2p\ ^1P_1$ are always larger than the ones to the level $1s2p\ ^3P_2$ and, in contrast to a slow increase in the former with the impact energy, the latter decreases quickly with the energy. Such a big difference between the behaviors of the total cross sections will ultimately affect angular emission of the $K\alpha_1$ line due to very different weights of its two fine-structure components. Apart from the total cross sections, their respective partial cross sections behave also very differently. For the $1s2p\ ^1P_1$ level, the partial cross sections to the magnetic substate $|M = 0\rangle$ increase with the impact energy within 2.0 times the excitation threshold and then decrease smoothly at higher energies, whereas the ones to the substates $|M = \pm 1\rangle$ keep increasing at all the energies considered. For the $1s2p\ ^3P_2$ level, in contrast, the corresponding partial cross sections behave with the impact energy in a similar way for all the substates $|M = 0\rangle$, $|M = \pm 1\rangle$, and $|M = \pm 2\rangle$. It should be noted that the relativistic distorted-wave theory is commonly expected to be able to give an accuracy of about 10% for total cross sections and 10–15% for partial ones for the presently considered very highly charged high- Z system. As the $K\alpha_1$ angular distribution is mainly dominated by relative values of total EIE cross sections to the $1s2p\ ^{1,3}P_{1,2}$ levels

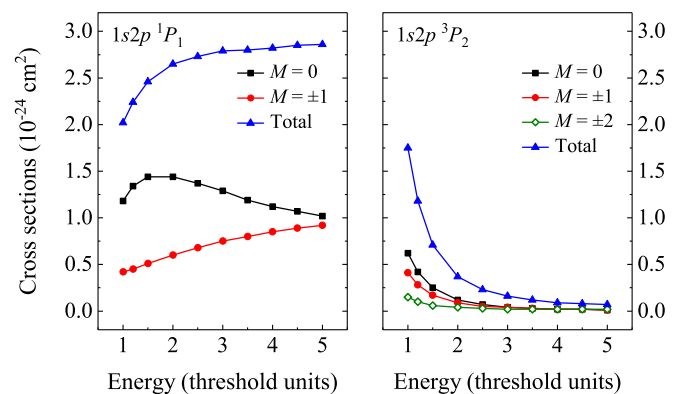


FIG. 1. Partial and total cross sections ($\times 10^{-24}\ \text{cm}^2$) for the EIE from the ground-state $1s^2\ ^1S_0$ to the magnetic substates of the excited energy levels $1s2p\ ^1P_1$ (left panel) and $1s2p\ ^3P_2$ (right) of heliumlike Ti^{79+} ions as functions of the impact electron energy in units of the excitation threshold 74.7501 keV of the $1s2p\ ^1P_1$ level. Please see Supplemental Material for the data used to generate this and the following figures [76].

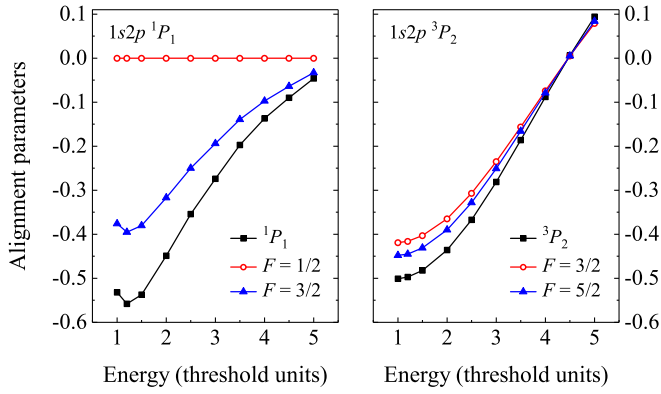


FIG. 2. Alignment parameters \mathcal{A}_2 of the fine-structure energy levels $1s2p\ ^1P_1$ (left panel) and $1s2p\ ^3P_2$ (right panel) as well as their corresponding hyperfine energy levels $1s2p\ ^1P_1$, $F = 1/2, 3/2$ and $1s2p\ ^3P_2$, $F = 3/2, 5/2$ of heliumlike spin-1/2 Tl^{79+} ions as functions of the impact electron energy in units of the excitation threshold 74.7501 keV.

via the weights of its two fine-structure components, such an accuracy still allows one to distinguish the hyperfine-induced effects obtained below for the $K\alpha_1$ angular distribution.

With the partial cross sections available, they can be readily utilized to calculate further the alignment parameters \mathcal{A}_2 of the two excited fine-structure energy levels as well as their corresponding hyperfine levels $1s2p\ ^1P_1$, $F = 1/2, 3/2$ and $1s2p\ ^3P_2$, $F = 3/2, 5/2$ of spin-1/2 Tl^{79+} ions by means of Eqs. (5), (6), and (11), as shown in Fig. 2 as functions of the impact electron energy. The alignment parameters of both the fine-structure levels $1s2p\ ^1,3P_{1,2}$ are found to be very sensitive to the impact electron energy. To be specific, for the level $1s2p\ ^1P_1$, the corresponding alignment parameter decreases from -0.532 to -0.532 within the impact energy of 5.0 times the excitation threshold. For the $1s2p\ ^3P_2$ level, in contrast, it behaves less and less aligned from -0.501 up to being fully unaligned at about 4.4 times the threshold and, then, becomes more aligned but in an opposite pattern at higher impact energies. As for the alignment parameters of the hyperfine levels, they behave quite similar to the ones of their respective fine-structure levels with increasing impact electron energy, although the hyperfine interaction weakens more or less the alignment of them and the alignment parameters of the hyperfine level $1s2p\ ^1P_1$, $F = 1/2$ are null at all the impact energies considered. Actually, it has been proven within the density matrix theory that atomic energy levels with total angular momentum $J \leq 1/2$ are certainly unpolarized, no matter how they are populated [53].

In Fig. 3, we present the effective anisotropy parameters β_2^{eff} of the $K\alpha_1$ lines radiated from heliumlike zero-spin Tl^{79+} ions as well as spin-1/2 $^{187}_{81}\text{Tl}^{79+}$ ($\mu_I = +1.550\mu_N$), $^{205}_{81}\text{Tl}^{79+}$ ($\mu_I = +1.638\mu_N$), and $^{207}_{81}\text{Tl}^{79+}$ ($\mu_I = +1.876\mu_N$) ions with large nuclear magnetic dipole moment μ_I [78] as functions of the impact electron energy. As can be seen clearly from the figure, the effective anisotropy parameters for both the zero-spin and spin-1/2 ions are strongly dependent on the impact electron energy. Moreover, the effects of the hyperfine interaction on the anisotropy parameters also depend remarkably on the impact electron energy. For low impact

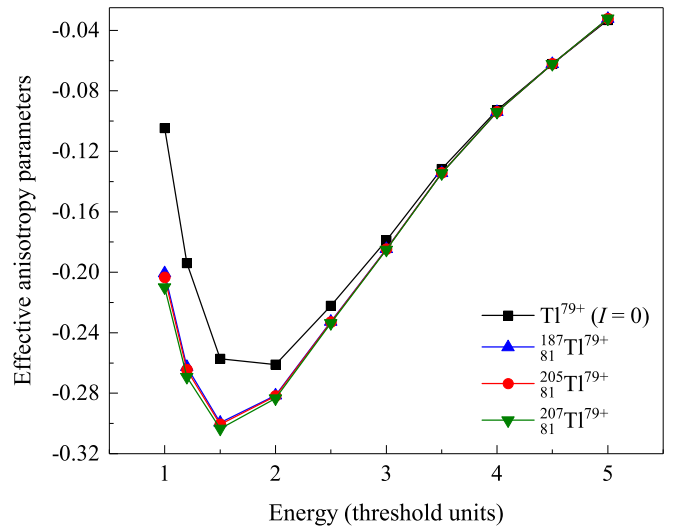


FIG. 3. Effective anisotropy parameters β_2^{eff} of the $K\alpha_1$ line radiated from heliumlike zero-spin Tl^{79+} (black line with squares) ions as well as spin-1/2 $^{187}_{81}\text{Tl}^{79+}$ ($\mu_I = +1.550\mu_N$, blue line with triangles), $^{205}_{81}\text{Tl}^{79+}$ ($\mu_I = +1.638\mu_N$, red line with circles), and $^{207}_{81}\text{Tl}^{79+}$ ($\mu_I = +1.876\mu_N$, olive line with inverted triangles) ions as functions of the impact electron energy in units of the excitation threshold 74.7501 keV.

energies, the hyperfine interaction contributes to enhancing the anisotropy of the $K\alpha_1$ lines; the lower the impact electron energy is, the more anisotropic the corresponding $K\alpha_1$ lines behave. At the impact energies near the excitation threshold, for example, the anisotropy parameters of the $K\alpha_1$ lines radiated from the spin-1/2 Tl^{79+} ions are enhanced by about 100%. Nevertheless, the contribution of the hyperfine interaction to the anisotropy parameters decreases quickly with increasing impact electron energy and, in particular, such a contribution vanishes for the impact energies higher than 3.0 times the excitation threshold. This is because for intermediate and high impact energies the $K\alpha_1$ line is predominantly determined by its fine-structure $E1$ component ($1s2p\ ^1P_1 \rightarrow 1s^2\ ^1S_0$) which cannot be affected by the hyperfine interaction at all as can be seen clearly from Eq. (12) and a quick increase in the weight \mathcal{N}_{E1} of the $E1$ component (i.e., with increasing impact energy \mathcal{N}_{E1} increases quickly from 0.60 at the impact energy of 1.0 times the excitation threshold to 0.98 at 5.0 times the threshold). For these spin-1/2 Tl^{79+} ions, moreover, the anisotropy parameters β_2^{eff} are found to be insensitive to the magnetic dipole moment μ_I even at low impact energies, and the reason is fully the same as the statement above, which is remarkably different from the anisotropy of the $M2$ ($1s2p\ ^3P_2 \rightarrow 1s^2\ ^1S_0$) lines following the EIE of spin-1/2 Tl^{79+} ions [52] and from the anisotropy of the $K\alpha_1$ lines following the REC of initially hydrogenlike spin-1/2 Sn^{49+} , Xe^{53+} , and Tl^{80+} ions [49,50].

By using the effective anisotropy parameters β_2^{eff} , the angular distribution of the $K\alpha_1$ lines can be readily determined for both the zero-spin and spin-1/2 Tl^{79+} ions. Figure 4 shows the angular distribution of the $K\alpha_1$ lines radiated from heliumlike zero-spin Tl^{79+} ions as well as spin-1/2 $^{187}_{81}\text{Tl}^{79+}$, $^{205}_{81}\text{Tl}^{79+}$, and $^{207}_{81}\text{Tl}^{79+}$ ions as functions of the impact electron energy.

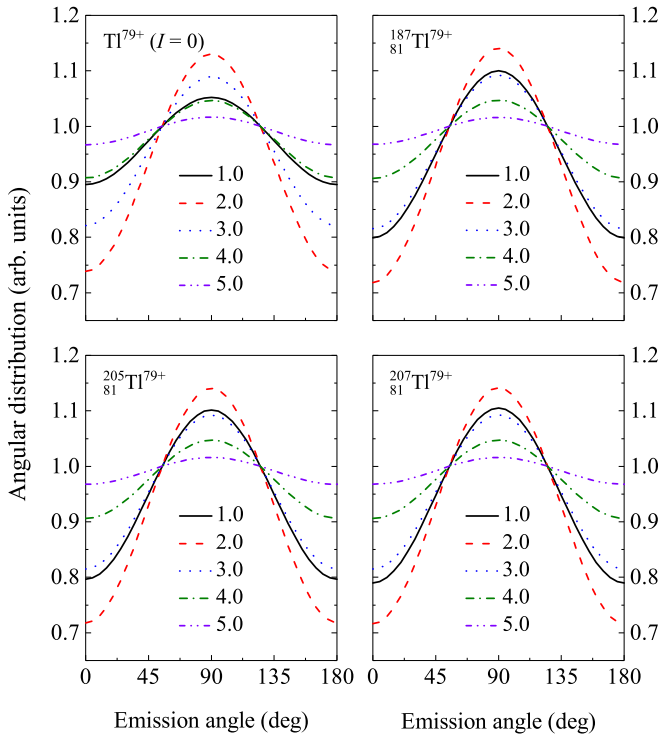


FIG. 4. Angular distribution of the $K\alpha_1$ line radiated from heliumlike zero-spin Tl^{79+} (top left panel) ions as well as spin-1/2 $^{187}_{81}\text{Tl}^{79+}$ (top right), $^{205}_{81}\text{Tl}^{79+}$ (bottom left), and $^{207}_{81}\text{Tl}^{79+}$ (bottom right) ions as functions of the impact electron energy. Results are presented for the impact electron energies 1.0 (black solid line), 2.0 (red dashed line), 3.0 (blue dotted line), 4.0 (olive dashed-dot line), and 5.0 (violet dashed-dot-dot line) in units of the excitation threshold 74.7501 keV.

Results are presented for the impact electron energies of 1.0, 2.0, 3.0, 4.0, and 5.0 times the excitation threshold 74.7501 keV. The $K\alpha_1$ angular distribution is similar for all zero-spin and spin-1/2 ions and has its maximum perpendicular to the incident electron beam (i.e., under $\theta = 90^\circ$) at all the impact energies. Moreover, the $K\alpha_1$ angular distribution is found to be rather sensitive to the impact energy for both the zero-spin and the spin-1/2 Tl^{79+} ions. At low impact energies and especially near the threshold the hyperfine interaction makes the $K\alpha_1$ angular distribution much more anisotropic, whereas it is hardly affected at intermediate and high energies.

To further explore the effects of the hyperfine interaction on angular emission properties of the $K\alpha_1$ lines radiated from the spin-1/2 Tl^{79+} ions, Fig. 5 shows the angular distribution of the $K\alpha_1$ lines as functions of the zero-spin and three spin-1/2 ions. Results are presented for two different impact energies. As seen obviously, near the excitation threshold the hyperfine interaction contributes to enhancing significantly the $K\alpha_1$ anisotropy for all the spin-1/2 Tl^{79+} ions, whereas at higher 3.0 times the threshold this effect vanishes quickly. Moreover, since the $E1$ component that cannot be affected by the hyperfine interaction dominates the corresponding $K\alpha_1$ emission at all the impact energies considered, the $K\alpha_1$ angular distribution is found to be insensitive to the magnetic dipole moment μ_I of the spin-1/2 Tl^{79+} ions.

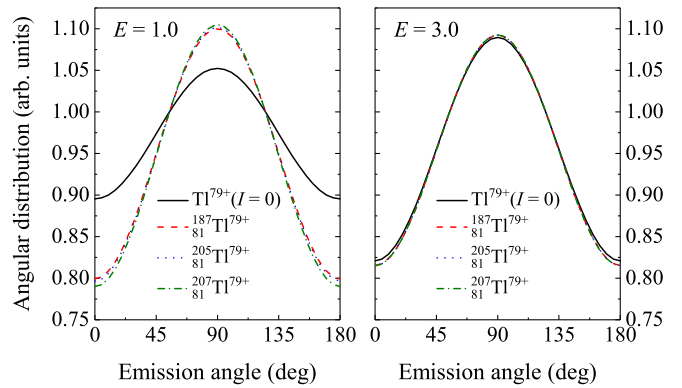


FIG. 5. Angular distribution of the $K\alpha_1$ line as functions of heliumlike zero-spin Tl^{79+} (black solid line) ions as well as spin-1/2 $^{187}_{81}\text{Tl}^{79+}$ (red dashed line), $^{205}_{81}\text{Tl}^{79+}$ (blue dotted line), and $^{207}_{81}\text{Tl}^{79+}$ (olive dashed-dot line) ions. Results are presented for two different impact electron energies 1.0 (left panel) and 3.0 (right) in units of the excitation threshold 74.7501 keV.

Based on these findings, we suggest that accurate measurements of the $K\alpha_1$ angular distribution at low impact energies could be employed as an effective tool to probe the hyperfine interaction in highly charged few-electron ions. To be detailed, if the $K\alpha_1$ angular distribution could be measured accurately for different spin-1/2 isotopes of thallium, the effect of the hyperfine interaction could be deduced from comparison with existing theoretical predictions. Although direct laser spectroscopy [79] is more effective than the present suggestion to probe the hyperfine interaction, admittedly, it is also an alternative scheme of stepping into this field. It is worth mentioning that the changes in the anisotropic angular distribution of the $K\alpha_1$ lines radiated from the spin-1/2 Tl^{79+} ions with respect to the $K\alpha_1$ angular distribution of the zero-spin Tl^{79+} ions are measurable by employing currently widely used x-ray detectors, such as high-purity germanium detectors and lithium-drifted silicon detectors [80], and, thus, could be carried out at both the electron beam ion trap and ion storage ring facilities [81,82]. Finally, it should be noted that since the energy separation of the two $1s2p\ ^1P_1$ and $1s2p\ ^3P_2$ levels is 60.918 eV and their widths are just 20.941 and 0.062 eV, respectively, the two fine-structure components of the $K\alpha_1$ lines can be resolved by using modern x-ray microcalorimeters [83,84]. Nevertheless, owing to high cost and especially strict measurement environments required by high-energy x-ray microcalorimeters, they are not very suitable to be used for x-ray angular distribution measurements, which require several detectors placed simultaneously at different emission angles.

IV. SUMMARY

To summarize, the EIE of heliumlike Tl^{79+} ions from their ground state to the $1s2p\ ^{1,3}P_{1,2}$ levels and the subsequent $K\alpha_1$ radiative decay have been studied within the framework of the density-matrix theory and the RDW theory. We aim to explore the effects of the hyperfine interaction on the $K\alpha_1$ angular distribution. To this aim, we have considered spin-1/2 $^{187}_{81}\text{Tl}^{79+}$, $^{205}_{81}\text{Tl}^{79+}$, and $^{207}_{81}\text{Tl}^{79+}$ ions with large μ_I and zero-spin Tl^{79+}

ions. Detailed calculations show that the hyperfine-induced effects on the $K\alpha_1$ angular distribution depend strongly on the impact electron energy. At low impact energies, the hyperfine interaction makes the $K\alpha_1$ angular distribution much more anisotropic, whereas it is hardly affected at intermediate and high energies. Such a rather strong energy dependence of the hyperfine-induced effects is resulted from a quick increase in the weight of the $E1$ component. Moreover, since the $E1$ component dominates the $K\alpha_1$ emission at all impact energies, the $K\alpha_1$ angular distribution is found to be insensitive to μ_I , which is remarkably different from the angular distribution of the $M2$ component following the EIE of spin-1/2 Tl^{79+} ions [52] and the $K\alpha_1$ angular distribution following the REC of initially hydrogenlike spin-1/2 Sn^{49+} , Xe^{53+} , and Tl^{80+} ions [49,50]. Finally, it is worth pointing out that the obtained hyperfine-induced effects on the $K\alpha_1$ angular distribution are measurable by utilizing present-day x-ray detectors and experimental facilities. We, therefore, suggest that accurate

measurements of the $K\alpha_1$ angular distribution at low impact energies could be used as an effective tool to probe the hyperfine interaction in highly charged few-electron ions.

ACKNOWLEDGMENTS

This work has been funded by the National Key R&D Program of China under Grant No. 2017YFA0402300. Z.W.W. thanks the National Natural Science Foundation of China under Grants No. 11804280 and No. 12174315, the Longyuan Youth Innovation and Entrepreneurship Talent Project of Gansu Province of China, the Youth Science and Technology Talent Promotion Project of Gansu Provincial Science and Technology Association of China under Grant No. GXH2020626-09, and the Major Program of the Research Ability Promotion Project for Young Scholars of Northwest Normal University of China under Grant No. NWNLUKQN2019-5.

-
- [1] J. L. Campbell, A. Perujo, W. J. Teesdale, and B. M. Millman, *Phys. Rev. A* **33**, 2410 (1986).
- [2] K. Jankowski and M. Polasik, *J. Phys. B: At., Mol. Opt. Phys.* **22**, 2369 (1989).
- [3] C. R. Bhuiya and H. C. Padhi, *Phys. Rev. A* **47**, 4885 (1993).
- [4] M. Ertugrul, Ö. Söğüt, Ö. Simsek, and E. Büyükkasap, *J. Phys. B: At., Mol. Opt. Phys.* **34**, 909 (2001).
- [5] J. P. Marques, F. Parente, and P. Indelicato, *J. Phys. B: At., Mol. Opt. Phys.* **34**, 3487 (2001).
- [6] T. Mukoyama, K. Taniguchi, and H. Adachi, *Phys. Rev. B* **34**, 3710 (1986).
- [7] V. L. Jacobs, G. A. Doschek, J. F. Seely, and R. D. Cowan, *Phys. Rev. A* **39**, 2411 (1989).
- [8] M. Polasik, *Phys. Rev. A* **41**, 3689 (1990).
- [9] C. Chenais-Popovics, C. Fievet, J. P. Geindre, I. Matsushima, and J. C. Gauthier, *Phys. Rev. A* **42**, 4788 (1990).
- [10] J. J. MacFarlane, P. Wang, J. Bailey, T. A. Mehlhorn, R. J. Dukart, and R. C. Mancini, *Phys. Rev. E* **47**, 2748 (1993).
- [11] A. S. Shlyaptseva, R. C. Mancini, and U. I. Safronova, *Phys. Scr.* **54**, 496 (1996).
- [12] J. Rządkiwicz, K. Słabkowska, M. Polasik, J. Starosta, E. Szymańska, K. Kozioł, M. Scholz, and N. R. Pereira, *Phys. Scr.* **2013**, 014083 (2013).
- [13] W. J. Kuhn and B. L. Scott, *Phys. Rev. A* **34**, 1125 (1986).
- [14] C. Ziener, I. Uschmann, G. Stobrawa, C. Reich, P. Gibbon, T. Feurer, A. Morak, S. Düsterer, H. Schwoerer, E. Förster, and R. Sauerbrey, *Phys. Rev. E* **65**, 066411 (2002).
- [15] B. Perny, J.-C. Dousse, M. Gasser, J. Kern, C. Rheme, P. Rymuza, and Z. Sujkowski, *Phys. Rev. A* **36**, 2120 (1987).
- [16] G. R. Babu, V. Gopalakrishna, M. L. N. Raju, K. Parthasaradhi, V. R. K. Murty, M. V. R. Murti, and K. S. Rao, *Phys. Rev. A* **36**, 386 (1987).
- [17] M. Deutsch, *Phys. Rev. A* **39**, 1077 (1989).
- [18] J. Kawai, Y. Nihei, Y. Z. Bai, K. Fujisawa, and Y. Gohshi, *Phys. Rev. A* **39**, 3686 (1989).
- [19] J. Ayers and J. Ladell, *Phys. Rev. A* **37**, 2404 (1988).
- [20] J. Kawai, C. Suzuki, H. Adachi, T. Konishi, and Y. Gohshi, *Phys. Rev. B* **50**, 11347 (1994).
- [21] B. Boschung, J.-C. Dousse, B. Galley, C. Herren, J. Hoszowska, J. Kern, C. Rhême, Z. Halabuka, T. Ludziejewski, P. Rymuza, Z. Sujkowski, and M. Polasik, *Phys. Rev. A* **51**, 3650 (1995).
- [22] A. Rousse, P. Audebert, J. P. Geindre, F. Fallières, J. C. Gauthier, A. Mysyrowicz, G. Grillon, and A. Antonetti, *Phys. Rev. E* **50**, 2200 (1994).
- [23] D. V. Rao, R. Cesareo, and G. E. Gigante, *Phys. Scr.* **54**, 325 (1996).
- [24] C. Chenais-Popovics, C. Fievet, J. P. Geindre, J. C. Gauthier, E. Luc-Koenig, J. F. Wyart, H. Pépin, and M. Chaker, *Phys. Rev. A* **40**, 3194 (1989).
- [25] J. P. Geindre, C. Chenais-Popovics, P. Audebert, C. A. Back, J. C. Gauthier, H. Pépin, and M. Chaker, *Phys. Rev. A* **43**, 3202 (1991).
- [26] H. Chen, B. Soom, B. Yaakobi, S. Uchida, and D. D. Meyerhofer, *Phys. Rev. Lett.* **70**, 3431 (1993).
- [27] V. Decaux, P. Beiersdorfer, S. M. Kahn, and V. L. Jacobs, *Astrophys. J.* **482**, 1076 (1997).
- [28] P. Palmeri, G. Boutoux, D. Batani, and P. Quinet, *Phys. Rev. E* **92**, 033108 (2015).
- [29] J. Kawai, K. Maeda, I. Higashi, M. Takami, Y. Hayasi, and M. Uda, *Phys. Rev. B* **42**, 5693 (1990).
- [30] Y. Muramatsu, M. Oshima, and H. Kato, *Phys. Rev. Lett.* **71**, 448 (1993).
- [31] T. Yaqoob, I. M. George, K. Nandra, T. J. Turner, P. J. Serlemitsos, and R. F. Mushotzky, *Astrophys. J.* **546**, 759 (2001).
- [32] J. J. Drake, B. Ercolano, and D. A. Swartz, *Astrophys. J.* **678**, 385 (2008).
- [33] X. W. Shu, T. Yaqoob, and J. X. Wang, *Astrophys. J.* **738**, 147 (2011).
- [34] R. R. Lindner, A. J. Baker, A. Beelen, F. N. Owen, and M. Polletta, *Astrophys. J.* **757**, 3 (2012).
- [35] G. Fabbiano, A. Siemiginowska, A. Paggi, M. Elvis, M. Volonteri, L. Mayer, M. Karovska, W. P. Maksym, G. Risaliti, and J. Wang, *Astrophys. J.* **870**, 69 (2019).

- [36] R. L. Placa, L. Stella, A. Papitto, P. Bakala, T. D. Salvo, M. Falanga, V. D. Falco, and A. D. Rosa, *Astrophys. J.* **893**, 129 (2020).
- [37] P. Chakraborty, G. J. Ferland, M. Chatzikos, F. Guzmán, and Y. Su, *Astrophys. J.* **901**, 68 (2020).
- [38] S. MacLaren, P. Beiersdorfer, D. A. Vogel, D. Knapp, R. E. Marrs, K. Wong, and R. Zasadzinski, *Phys. Rev. A* **45**, 329 (1992).
- [39] P. Indelicato and E. Lindroth, *Phys. Rev. A* **46**, 2426 (1992).
- [40] K. Widmann, P. Beiersdorfer, V. Decaux, and M. Bitter, *Phys. Rev. A* **53**, 2200 (1996).
- [41] L. Zhang, G. Jiang, L. Hao, and B. Deng, *Phys. Scr.* **83**, 025302 (2011).
- [42] M. H. Mendenhall, A. Henins, L. T. Hudson, C. I. Szabo, D. Windover, and J. P. Cline, *J. Phys. B: At., Mol. Opt. Phys.* **50**, 115004 (2017).
- [43] J. W. Dean, H. A. Melia, C. T. Chantler, and L. F. Smale, *J. Phys. B: At., Mol. Opt. Phys.* **52**, 165002 (2019).
- [44] N. Maskil and M. Deutsch, *Phys. Rev. A* **38**, 3467 (1988).
- [45] M. Deutsch, G. Hölzer, J. Härtwig, J. Wolf, M. Fritsch, and E. Förster, *Phys. Rev. A* **51**, 283 (1995).
- [46] A. M. Costa, M. C. Martins, J. P. Santos, P. Indelicato, and F. Parente, *J. Phys. B: At., Mol. Opt. Phys.* **40**, 57 (2006).
- [47] J. R. Henderson, P. Beiersdorfer, C. L. Bennett, S. Chantrenne, D. A. Knapp, R. E. Marrs, M. B. Schneider, K. L. Wong, G. A. Doschek, J. F. Seely, C. M. Brown, R. E. LaVilla, J. Dubau, and M. A. Levine, *Phys. Rev. Lett.* **65**, 705 (1990).
- [48] A. Surzhykov, Y. Litvinov, T. Stöhlker, and S. Fritzsche, *Phys. Rev. A* **87**, 052507 (2013).
- [49] Z. W. Wu, A. Surzhykov, and S. Fritzsche, *Phys. Rev. A* **89**, 022513 (2014).
- [50] Z. W. Wu, A. Surzhykov, and S. Fritzsche, *Phys. Rev. A* **91**, 056502 (2015).
- [51] Z. W. Wu, S. Fritzsche, and A. Surzhykov, *Phys. Scr.* **2015**, 014029 (2015).
- [52] Z. W. Wu, Z. Q. Tian, J. Jiang, C. Z. Dong, and S. Fritzsche, *Phys. Rev. A* **102**, 042813 (2020).
- [53] V. V. Balashov, A. N. Grum-Grzhimailo, and N. M. Kabachnik, *Polarization and Correlation Phenomena in Atomic Collisions* (Kluwer Academic, New York, 2000).
- [54] A. Surzhykov, U. D. Jentschura, T. Stöhlker, and S. Fritzsche, *Phys. Rev. A* **74**, 052710 (2006).
- [55] A. Surzhykov, U. D. Jentschura, T. Stöhlker, and S. Fritzsche, *Phys. Rev. A* **73**, 032716 (2006).
- [56] H. L. Zhang, D. H. Sampson, and R. E. H. Clark, *Phys. Rev. A* **41**, 198 (1990).
- [57] H. L. Zhang and D. H. Sampson, *Phys. Rev. A* **66**, 042704 (2002).
- [58] Z. W. Wu, J. Jiang, and C. Z. Dong, *Phys. Rev. A* **84**, 032713 (2011).
- [59] Z. W. Wu, C. Z. Dong, and J. Jiang, *Phys. Rev. A* **86**, 022712 (2012).
- [60] C. Ren, Z. W. Wu, J. Jiang, L. Y. Xie, D. H. Zhang, and C. Z. Dong, *Phys. Rev. A* **98**, 012711 (2018).
- [61] Z. W. Wu, M. M. Zhao, C. Ren, C. Z. Dong, and J. Jiang, *Phys. Rev. A* **101**, 022701 (2020).
- [62] M. K. Inal and M. Benmouna, *Phys. Rev. A* **91**, 056501 (2015).
- [63] F. A. Parpia, C. F. Fischer, and I. P. Grant, *Comput. Phys. Commun.* **94**, 249 (1996).
- [64] I. P. Grant, *Relativistic Quantum Theory of Atoms and Molecules: Theory and Computation* (Springer-Verlag, New York, 2007).
- [65] J. Jiang, C. Z. Dong, L. Y. Xie, and J. G. Wang, *Phys. Rev. A* **78**, 022709 (2008).
- [66] S. Fritzsche, *Comput. Phys. Commun.* **183**, 1525 (2012).
- [67] S. Fritzsche, *Comput. Phys. Commun.* **240**, 1 (2019).
- [68] C. J. Bostock, D. V. Fursa, and I. Bray, *Phys. Rev. A* **80**, 052708 (2009).
- [69] S. Fritzsche, A. Surzhykov, and T. Stöhlker, *Phys. Rev. Lett.* **103**, 113001 (2009).
- [70] P. Indelicato, F. Parente, and R. Marrus, *Phys. Rev. A* **40**, 3505 (1989).
- [71] K. T. Cheng, M. H. Chen, and W. R. Johnson, *Phys. Rev. A* **77**, 052504 (2008).
- [72] W. R. Johnson, K. T. Cheng, and D. R. Plante, *Phys. Rev. A* **55**, 2728 (1997).
- [73] W. Johnson, *Can. J. Phys.* **89**, 429 (2011).
- [74] L. Głowacki, *Atom. Data Nucl. Data Tables* **133-134**, 101344 (2020).
- [75] G. W. Drake, *Can. J. Phys.* **66**, 586 (1988).
- [76] See Supplemental Material at <http://link.aps.org/supplemental/10.1103/PhysRevA.104.062814> for the data used to generate this and figures.
- [77] K. J. Reed and M. H. Chen, *Phys. Rev. A* **48**, 3644 (1993).
- [78] N. J. Stone, *At. Data Nucl. Data Tables* **90**, 75 (2005).
- [79] J. Ullmann, Z. Andelkovic, C. Brandau, A. Dax, W. Geithner, C. Geppert, C. Gorges, M. Hammen, V. Hannen, S. Kaufmann *et al.*, *Nat. Commun.* **8**, 15484 (2017).
- [80] B. Yang, D. Yu, C. Shao, X. Cai, Z. Wu, L. Xie, K. N. Lyashchenko, Y. S. Kozhedub, K. Ma, Y. Xue, W. Wang, M. Zhang, J. Liu, R. Lu, Z. Song, Y. Wu, F. Ruan, Y. Zhang, C. Dong, and Z. Yang, *Phys. Rev. A* **104**, 032815 (2021).
- [81] G. Weber, H. Bräuning, A. Surzhykov, C. Brandau, S. Fritzsche, S. Geyer, S. Hagmann, S. Hess, C. Kozhuharov, R. Märtin, N. Petridis, R. Reuschl, U. Spillmann, S. Trotsenko, D.F.A. Winters, and T. Stöhlker, *Phys. Rev. Lett.* **105**, 243002 (2010).
- [82] P. Amaro, C. Shah, R. Steinbrügge, C. Beilmann, S. Bernitt, J. R. C. López-Urrutia, and S. Tashenov, *Phys. Rev. A* **95**, 022712 (2017).
- [83] S. Kraft-Bermuth, V. Andrianov, A. Bleile, A. Echler, P. Egelhof, P. Grabitz, S. Ilieva, O. Kiselev, C. Kilbourne, D. McCammon *et al.*, *J. Phys. B: At. Mol. Opt. Phys.* **50**, 055603 (2017).
- [84] C. Pies, S. Schäfer, S. Heuser, S. Kempf, A. Pabinger, J. Porst, P. Ranitsch, N. Foerster, D. Hengstler, A. Kampkötter *et al.*, *J. Low Temp. Phys.* **167**, 269 (2012).